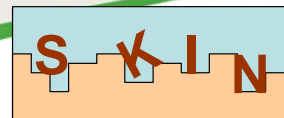




EUROPEAN
COMMISSION

European
Research Area



Report on adding uptake kinetics and surface entrapment to geochemical models.

Modelling code extensions and test results.

**SLOW PROCESSES IN CLOSE-TO-EQUILIBRIUM CONDITIONS FOR
RADIONUCLIDES IN WATER/SOLID SYSTEMS OF RELEVANCE TO NUCLEAR
WASTE MANAGEMENT**

SKIN

DELIVERABLE D4.2

COLLABORATIVE PROJECT (CP)

Grant agreement N°.: FP7-269688

Submitting organizations: PSI

Authors: Dmitrii A. Kulik, Bruno M.J. Thien

Due date of deliverable: Project Month 34

Actual submission: Project Month 36

Start date of the project: 01 January 2011

Duration: 36 months

Project co-funded by the European Commission under the Seventh Framework Programme of the European Atomic Energy Community (Euratom) for nuclear research and training activities (2007 to 2011)		
Dissemination Level		
PU	Public	×
RE	Restricted to a group specified by the partners of the project	
CO	Confidential, only for partners of the project	

WP4 TASK 1: ADDING UPTAKE KINETICS AND SURFACE ENTRAPMENT TO GEOCHEMICAL MODELS. MODELLING CODE EXTENSIONS AND TEST RESULTS

Dmitrii A. Kulik^{1*}, Bruno M.J. Thien¹

¹Paul Scherrer Institut, Laboratory for Waste Management (LES), 5232 Villigen PSI (CH)

* Corresponding author: dmitrii.kulik@psi.ch

Summary

Our work was aimed at the development of a new partial equilibrium approach to geochemical modeling of the slow uptake of radionuclides in host mineral solid solutions, verified against the literature experimental data. In this work, the extensions of the TKinMet code library of the GEM-Selektor package, necessary for the simulation of kinetically-controlled mineral-water interactions, have been implemented. This is a pre-requisite for using kinetic models efficiently in reactive transport codes coupled with the Gibbs Energy Minimization software (GEMS). In the framework of SKIN project, a comparative study of available models of trace element uptake kinetics upon host mineral precipitation has been performed. The resulting “unified uptake kinetics model” (UUKM) for trace element incorporation upon the host mineral growth (*Thien, Kulik and Curti, 2013*), initially tested using GEMS process simulator scripts, has also been implemented in TKinMet library of the GEM-Selektor code package (<http://gems.web.psi.ch>). The extended code has been tested using the literature data for the rate-dependent uptake of trace elements upon calcite growth.

The first part of this report provides a description of theory and principles used in modelling code extensions, leaving most technical details to the runtime GEM-Selektor help database as part of the GEM-Selektor v.3.3 code prototype. The second part of the report shows how the software extensions have been tested, firstly on two examples of precipitation kinetics of portlandite and calcite, and secondly, against some experimental data for Sr and Cd uptake kinetics in calcite. Geochemically important effects such as the depletion in a closed system and the arbitrarily changing composition of the open system, as reproduced by the implemented kinetic and uptake models, are illustrated by simulations of (hypothetical) variations of Sr uptake in calcite precipitating from seawater. The tests show that the TKinMet code library extensions for mineral-water reaction kinetics and trace element uptake into solid solutions in aqueous systems within the GEM-Selektor code comprise an efficient modelling tool of potentially wide applicability in aquatic chemistry, chemical engineering, and (nuclear) waste geochemistry.

Introduction

Aquatic chemical systems at Earth surface conditions rarely achieve the truly reversible equilibrium state. No mineral solid precipitates or dissolves instantly; at room temperature T and pressure P , some coarse-crystalline phases are almost unreactive; others (e.g. clays) dissolve relatively fast, but do not precipitate. Particulate solid nanophases with large specific surface areas are metastable with respect to their bulk counterparts due to the positive surface free energy contribution (*Wu and Nancollas, 1999; Navrotsky, 2011*). Hence, the phase metastability and solid-aqueous reaction kinetics must be accounted for in any realistic chemical thermodynamic model of a complex aquatic system. This becomes critical when chemical thermodynamic models are embedded in reactive transport simulations, performed using the coupled codes such as PHAST (*Parkhurst et al., 2010*) or OpenGeoSys-GEM (*Shao et al., 2009*) that combine a fluid transport model with the chemical speciation solver, using a discretization of the system in space (many small enough control volumes) and in time (many small enough time steps Δt). In such simulations, based on the *principles of local and partial equilibrium*, the missing or incorrect account for mineral-aqueous reaction kinetics may often lead to intractably small time steps and/or to completely unrealistic predictions.

1. Methods of GEM simulations of mineral-aqueous reaction kinetics

1.1. Local and partial equilibrium

The *local equilibrium* is assumed to take place in each control volume, according to the assigned bulk system composition and the thermodynamic parameters of state (pressure P , temperature T , surface area A of phases). The *partial equilibrium* occurs if some components in some phases cannot reach their equilibrium amounts because of the *additional metastability restrictions* (AMR). All phases and components without AMR take part in the achievement of the partial equilibrium state under the mass balance common to the whole system.

If a chemical speciation solver can handle AMRs, such as the GEM-Selektor (*Karpov et al., 2001; Kulik et al., 2013; Wagner et al., 2012*), it can be directly employed for simulating the kinetics of a time-dependent chemical process by setting each AMR as a function of the time step duration Δt , the time variable t , the surface area $A_{k,t}$ of k -th solid phase, and the net molar kinetic rate $R_{n,k,t}$ (details are given below). In principle, AMRs may also depend on a linkage of the specific surface of one phase (e.g. an overgrowth, adsorbed layer) to the volume or surface area of another, “seed”, “substrate” or “adsorbent” phase, which may even be inert, or may have its own kinetics.

In a stepwise simulation, the mole amount $n_{k,t+\Delta t}$ of the solid at time $t+\Delta t$ is set by the upper AMR $\bar{n}_{k,t+\Delta t}$ for precipitation or by the lower AMR $\underline{n}_{k,t+\Delta t}$ for dissolution:

$$\begin{aligned}\bar{n}_{k,t+\Delta t} &= n_{k,t} + A_{k,t} R_{n,k,t} \Delta t \quad \text{if } \log_{10} \Omega_k > \varepsilon \\ \underline{n}_{k,t+\Delta t} &= n_{k,t} - A_{k,t} R_{n,k,t} \Delta t \quad \text{if } \log_{10} \Omega_k < -\varepsilon\end{aligned}\quad (1),$$

where $0 < \varepsilon < 10^{-5}$ is a numerical tolerance. The direction of change depends on the sign of the logarithmic phase stability index $\log_{10} \Omega_k$ (explained below). The surface area of the k -th solid phase is obtained as $A_{k,t} = A_{S,k} M_{M,k} n_{k,t}$, where $A_{S,k}$ is the specific surface area ($\text{m}^2 \text{kg}^{-1}$); $M_{M,k}$ is the molar mass (kg mol^{-1}), and $n_{k,t}$ is the current amount (mol) of the k -th phase.

The implementation of metastability and kinetics differs from code to code; so far, there is no conventional data structure for kinetic parameters. Large literature exists on experimental data and kinetic rate laws and parameters of mineral-aqueous reactions (*e.g. Teng et al., 2000; Schott et al., 2009, 2012*), with a generally better understanding of dissolution compared to that for precipitation and nucleation. Because the experimental rate constants are typically normalized per unit area, they must be scaled by the current reactive surface area of the mineral, which depends on many factors, some of them are external to the chemical system, and some related to the particle/pore morphology, initial size distributions, and surface roughness. At present, the determination of reactive surface areas is perhaps the most important knowledge gap (*Marini et al., 2000; Mironenko and Zolotov, 2012; Scislawski and Zuddas, 2010*), related in reactive transport modeling to the impact of porosity changes on transport and kinetic parameters. Many kinetic rate laws contain the activity product term related to a particular reaction mechanism, catalysis, inhibition, etc. (*Schott et al., 2012; Palandri and Kharaka, 2004*). Kinetic rates also depend on the *affinity term* based on the *phase saturation index* Ω_k ; particular forms of this term reflect different nucleation, growth or dissolution mechanisms.

1.2. Gibbs energy minimization (GEM) method

The GEM IPM (interior points method) algorithm (*Kulik et al., 2013*), implemented in the GEM Software (GEMS), has a great potential for thermodynamic modeling of mineral-water reaction kinetics because it can directly handle the metastability restrictions. In the GEM IPM, the chemical system is defined by a bulk composition vector, $n^{(b)}$, specifying the input amounts of chemical elements and charge; the standard molar Gibbs energies of all dependent components (species), g° , at T, P of interest; the parameters of (non)ideal models of mixing in solution phases (*Wagner et al., 2012*), needed to calculate activity coefficients λ_j of species indexed with j ; and the optional AMRs. After each run, the GEM *primal* (speciation vector $\hat{n}^{(x)}$) and the *dual* (vector $\hat{u}^{(b)}$) of chemical potentials of chemical elements and charge) results provide concentrations and activities of all aqueous species, as well as activities and amounts of all components in all other phases. The stability index Ω_k of any phase, even of that absent from the mass balance, is found as a *dual-thermodynamic* estimate of the sum of (anticipated) mole fractions \hat{x}_j of all phase components:

$$\Omega_k = \sum_j \hat{x}_j = \sum_j \exp\left(\hat{\eta}_j - \frac{g_j^o}{RT} - \ln \lambda_j - \Xi_k\right) \quad (2)$$

where the index j runs over all components in the phase; R is the universal gas constant; Ξ_k is a term for converting species concentration into the common mole fraction scale (e.g. $\ln P$ for gases; $\ln 55.5085$ for aqueous species); and $\hat{\eta}_j$ stands for the *dual-solution chemical potential*

$$\hat{\eta}_j = \sum_i \mathbf{a}_{ij} \hat{\mu}_i^{(b)} \quad (3)$$

where index i runs over all chemical elements and charge, and \mathbf{a}_{ij} is the formula stoichiometry coefficient of i -th element in j -th species (e.g. 2 for O in SiO_2).

In the GEM IPM algorithm, the Ω_k index (eq 2) is used as a *criterion of stability* for any phase. If, numerically, $-0.01 < \log_{10}\Omega_k < 0.01$ then the positive or zero amount of this phase is in equilibrium with the rest of the system. If $\log_{10}\Omega_k < -0.01$ then the phase is unstable (the rest of the system is under-saturated to this phase), but may be kept in a positive amount in the mass balance by the lower AMR(s) \underline{n}_j set on some or all of its components. If $\log_{10}\Omega_k > 0.01$ then the phase is over-stable (the rest of the system is oversaturated to this phase) because the positive or zero upper AMR(s) \bar{n}_j were set on some of its components from above.

Taken together, the GEM IPM output phase stability index Ω_k together with the input lower- \underline{n}_j and upper \bar{n}_j AMRs make the GEM-Selektor code a versatile tool for modelling various kinds of kinetics and metastability, represented as the sequences of partial (restricted) equilibrium states. Thus, lower-AMRs allow stepwise simulation of *dissolution* of a mineral as long as its stability index $\Omega_k < 1$; upper-AMRs allow stepwise simulation of mineral *precipitation* as long as $\Omega_k > 1$. Setting AMRs as a function of time according to the chosen kinetic rate law allows the GEM software to simulate the kinetics of mineral-aqueous reactions and trace element uptake. The more ample information about the mineral-aqueous reaction is available from the experiment the more accurate and specific form of the rate equation can be applied to the system of interest.

1.3. The TKinMet library of models of mineral-aqueous reaction kinetics

Some kinetic rate equations for dissolution, precipitation, and trace element uptake in solid solutions have been implemented in the TKinMet code library used in GEM-Selektor and GEMS3K codes. Eventually, with this library, GEMS will become a general and flexible software tool, extending and superseding the existing (geo)chemical models and codes capable of kinetic simulations (*Parkhurst and Appelo 1999; Made et al., 1994; Fritz et al., 2009; Mironenko and Zolotov, 2012*). In the TKinMet library, mineral-water interaction kinetic rate laws are considered in a traditional form derived from (*Lasaga, 1998; Palandri and Kharaka, 2004; Schott et al., 2012*):

$$\frac{dn_k}{dt} = A_{k,t} R_{n,k,t} = -A_{k,t} \sum_r^{N(r)_k} \left\{ \theta_{k,r,t} f(\kappa, E)_{k,r} f(\Pi a)_{k,r,t} f(\Omega)_{k,r,t} \right\} \quad (4)$$

where k is the index of solid phase of interest (pure solid or solid solution); n_k is the mole amount of k -th phase at time t ; $A_{k,t}$ is the current surface area of the phase in m^2 ; $R_{n,k,t}$ is the total precipitation or dissolution rate (in $\text{mol m}^{-2}\text{s}^{-1}$); $N(r)_k$ is the number of parallel reactions or pathways that affect the amount of k -th phase; r is the index of a reaction or a pathway (dissolution, nucleation, and precipitation can be treated as different parallel reactions); $\theta_{k,r,t}$ is the effective fraction of surface area of k -th phase assigned to the r -th parallel reaction. Time-dependent parameters $A_{k,t}$ and $\theta_{k,r,t}$ may either depend on a built-in model of particle size/area evolution or be externally controlled from the mass transport code. In eq (4),

$$f(\kappa, E) = \kappa_{k,r}^o \Lambda_{k,r} e^{\frac{-E_{k,r}}{RT}} \quad (5)$$

is the *reaction rate constant term* including the temperature correction, where: $\kappa_{k,r}^o$ is the rate constant at reference temperature (25 C) in $\text{mol m}^{-2}\text{s}^{-1}$ or other appropriate units; the sign convention of $\kappa_{k,r}^o$ is: positive sign for dissolution and negative for precipitation; T is the temperature in K; $\Lambda_{k,r}$ is the Arrhenius factor (1 by default); R is the universal gas constant ($8.31451 \text{ J K}^{-1} \text{ mol}^{-1}$); and $E_{k,r}$ is the activation energy (J mol^{-1}) of r -th «parallel reaction». The expression $e^{\frac{-E_{k,r}}{RT}}$ in eq (5) is sometimes represented in another form $e^{\frac{-E_{k,r}^*}{R} \left(\frac{1}{T} - \frac{1}{298.15} \right)}$ involving the reference temperature 298.15 K (*Palandri and Kharaka, 2004*). Both are connected as:

$$\Lambda_{k,r} \cdot e^{\frac{-E_{k,r}}{RT}} = \Lambda_{k,r}^* \cdot e^{\frac{-E_{k,r}^*}{R} \left(\frac{1}{T} - \frac{1}{298.15} \right)} \quad \text{or} \quad \Lambda_{k,r} = \Lambda_{k,r}^* \cdot e^{\frac{-E_{k,r}^*}{R \cdot 298.15}} \quad (6)$$

under the assumption that $E_{k,r}^* = E_{k,r}$.

In eq (4),

$$f(\Pi a)_{k,r} = I^{b_{I,k,r}} \text{pH}^{b_{\text{pH},k,r}} \text{pe}^{b_{\text{pe},k,r}} \text{Eh}^{b_{\text{Eh},k,r}} \left(\prod_j^{n(j)_{k,r}} a_{j,k,r}^{b_{j,k,r}} \right)^{p_{k,r}} \quad (7)$$

is the current (at time t) *activity product term*, combined to accommodate most of the literature rate laws, where: I is the (effective molal) ionic strength; $b_{I,k,r}$ is the related empirical parameter; $b_{\text{pH},k,r}$ is the empirical parameter related to pH; $b_{\text{pe},k,r}$ is the parameter related to pe; $b_{\text{Eh},k,r}$ is the parameter related to Eh, V; $p_{k,r}$ is the «reaction order» parameter; $n(j)_{k,r}$ is the number of (aqueous or gaseous or surface) species from other reacting phases involved; $a_{j,k,r}$ is the activity (fugacity) of j -th species ($a_{\text{H}^+} = 10^{-\text{pH}}$, $a_e = 10^{-\text{pe}}$); $b_{j,k,r}$ is the (reaction stoichiometry coefficient) parameter. Note that in eq (6), any term can be disabled if the respective power coefficient is set to the default value of zero.

Finally, in eq (4), $f(\mathbf{\Omega})_{k,r}$ is the affinity term for r -th reaction, which can take several different forms, all using the current (at time t) k -th phase stability index $\mathbf{\Omega}_k$ (eq 2). Different forms of the affinity term (see section 1.7) reflect different crystal growth or dissolution mechanisms. The classic affinity term is taken in the form $(1 + u_{k,r} - \Omega_k^{q_{k,r}})^{m_{k,r}}$ where $q_{k,r}$ and $m_{k,r}$ are the reaction order parameters (default value 1; $m_{k,r} = 0$ disables the affinity term); and $u_{k,r}$ is the empirical parameter (default value 0).

In eq. (4), the net rate $R_{n,k,t}$ is taken in $\text{mol}\cdot\text{m}^{-2}\cdot\text{s}^{-1}$ by default. However, in modern models of mineral dissolution or growth (e.g. **Wolthers, 2012; Nielsen et al., 2013**), the mean orthogonal *velocity of surface propagation* $R_{L,k,t}$ in $\text{m}\cdot\text{s}^{-1}$ is considered. $R_{L,k,t}$ relates to $R_{n,k,t}$ as

$$R_{L,k,t} = V_{M,k} R_{n,k,t} = \frac{M_{M,k}}{\rho_k} R_{n,k,t} \quad (8)$$

where $V_{M,k}$ is the mineral molar volume in $\text{m}^3\cdot\text{mol}^{-1}$; $M_{M,k}$ is the molar mass of the phase in $\text{kg}\cdot\text{mol}^{-1}$; and ρ_k is the phase density in $\text{kg}\cdot\text{m}^{-3}$.

Specific surface area of the mineral is defined as $A_{S,k} = A_k/m_k$ (in $\text{m}^2\cdot\text{kg}^{-1}$) or $A_{V,k} = A_k/V_k$ (in m^{-1}). Upon growth or dissolution, both $A_{S,k}$ and $A_{V,k}$ values vary with time because of changing particle size, shape, and surface roughness. Hence, in kinetic simulations, reactive surface areas must be corrected after each time step, either internally in TKinMet library functions, or externally controlled by the reactive transport model. In the simplest case, currently implemented in the TKinMet library, for particles of similar size and shape, assuming no density change of the mineral upon growth and no other second-order effects,

$$A_{V,k,t} = A_{V,k,t-\Delta t} \frac{\psi_{k,t-\Delta t}}{\psi_{k,t}} \frac{d_{VS,k,t-\Delta t}}{d_{VS,k,t-\Delta t} + 2R_{L,k,t}\Delta t} \quad (9)$$

where $A_{V,k,t}$ is the current specific surface area; $d_{VS,k}$ is the mean particle volume-surface diameter; and $R_{L,k}$ is the current linear rate from eq (8). As a shape factor, we use the *sphericity* coefficient $0 < \psi_k \leq 1$ (**Wadell, 1935**), defined as:

$$\psi_k = \pi^{1/3} \frac{(6V_p)^{2/3}}{A_p} = \frac{6V_p}{d_p A_p} \quad (10)$$

where $d_p = d_{VS,k} = \frac{6}{\psi_k} \frac{V_p}{A_{V,k}}$ is the *estimated particle size*; $V_p = \frac{1}{6}\pi d_p^3$ is the *mean particle volume*; and $A_p = A_k \frac{V_p}{V_k}$ is the *mean particle surface area*. Sphericity (eq 10) is the external parameter of the kinetics model; the initial ψ_0 value must be defined together with other initial parameters at the beginning of simulations. From simple geometric considerations,

perfect mineral crystals must have sphericity about 0.8 ± 0.1 ; values below 0.7 apply to thin platelets or to rough surfaces of aggregate particles.

In eq (9), the evolution of sphericity describes the impact of changing morphology and surface roughness on the variation of (reactive) specific surface area and thus onto dissolution or precipitation rates of the solid. Again, this evolution can be controlled externally (from the mass transport model), or represented as a function of some system parameters, for instance

$$\psi_k(t) = \psi_{0,k} + \psi_{1,k}u + \psi_{2,k}u^2 + \dots \quad (11)$$

where $\psi_{0,k}$, $\psi_{1,k}$, $\psi_{2,k}$, ... are the empirical coefficients, and the u variable can be e.g. the phase stability index $u = \log_{10} \Omega_{k,t}$, the relative change of phase amount $u = (n_{k,t} - n_{k,0}) / n_{k,0}$, or the function of growth rate $R_{L,k,t}$, of temperature T , or of other system variables.

At the same stoichiometry and chemical potential, the activity of any j -th component and the stability index of the whole phase Ω_k will depend on the value(s) of its standard-state per-mole Gibbs energy g_j^0 (see eq 2). In fact, the g_j^0 parameter can also reflect the differences in stability for polymorphic modifications of the same compound (e.g. amorphous calcium carbonate, vaterite, aragonite, calcite), as well as the impact of surface free energy (or interface tension) γ , or other energy factors. Therefore, we consider the g_j^0 term with its possible modifications and extensions as a main spot to connect thermodynamic models, kinetic rates, and crystallization pathways, in addition to the $\psi_{k,t} = f(t, n, \Omega, \dots)$ function and $\theta_{k,r,t}$ parameters for parallel reactions.

In the TKinMet library, some parameters, e.g. the dissolution rate constant, the activation energy, the reaction type and order constants for parallel reactions, are considered as chemical properties of the solid phase, kept in the respective phase definition record in GEMS project database. Other parameters, such as the shape factor function $\psi_{k,t} = f(t, n, \Omega, \dots)$ and reactive fraction $\theta_{k,r}$ of surface area assigned to r -th parallel reaction, are related to evolving particle or pore size and shape distributions. Such parameters can be set externally, e.g. on the basis of assumptions of the reactive-transport or the crystallization pathway model. These parameters with their variation should generally come into TKinMet calculations from the process simulator or from the transport part of the coupled reactive transport code.

1.4. Aqueous - solid solution systems

For solid solutions, in the next partial equilibrium state at time $t + \Delta t$, the TKinMet code will split the new AMRs for the total amount of phase $\bar{n}_{k,t+\Delta t}$ into AMRs to the end members $\bar{n}_{j,t+\Delta t}^{(x)}$ (the symbols here refer to both upper- and lower AMR cases in eqs (1)). There are several ways of such splitting, depending on a particular dissolution, precipitation, or nucleation process (this part of TKinMet code is still under development). For example, the

dissolution of a sparingly-soluble solid solution usually occurs stoichiometrically (*Glynn and Reardon, 1990*), which can be represented by changing AMRs for end members proportional to their mole fractions:

$$\begin{aligned} \underline{n}_{k,t+\Delta t} &= n_{k,t} + A_{k,t} R_{n,k,t} \Delta t \quad \text{if} \quad \log_{10} \Omega_k < -\varepsilon \\ \underline{n}_{j,t+\Delta t}^{(x)} &= n_{j,t}^{(x)} + x_{j,t} (\underline{n}_{k,t+\Delta t} - n_{k,t}) \end{aligned} \quad (12)$$

Here, $x_{j,t}$ is the current mole fraction of j -th end member, and the index j runs over all end members in the solid solution phase. The impact of another (secondary) phase precipitation on the dissolution rate $R_{n,k,t}$ is accounted for by changes in the saturation index $\Omega_{k,t}$ or explicitly by augmenting the shape factor $\psi_{k,t}$ or the reactive area fractions $\theta_{k,r,t}$. For nucleation and growth, such relationships become complex (*Prieto, 2009*) because such processes depend on the contribution of surface free energies that, in turn, depends on particle size and curvature.

In the present contribution, the case of uptake of a trace element (Tr) into a binary solid solution with the host element (Hc) is presented, as this case was considered in the SKIN project. Here, the rate law for the host mineral is applied to the whole solid solution phase, and used as the basis for the uptake kinetics model discussed previously in the WP4 Task 1 mid-term report (*Thien et al., 2013; in revision*).

The distribution of Tr between the aqueous and the solid solution relative to Hc is described by the fractionation coefficient $\Delta_{Tr,Hc}$, which is the ratio of two distribution ratios R_d :

$$\Delta_{Tr,Hc} = \frac{R_d(Tr)}{R_d(Hc)} \quad (13)$$

The distribution ratio is defined as the ratio of component concentration in the solid to that in the aqueous phase. Taking mole fraction x for the solid and total dissolved molality $[\]$ for the aqueous part as concentrations:

$$\Delta_{Tr,Hc} = \left(\frac{x_{Tr}}{[Tr]} \right) / \left(\frac{x_{Hc}}{[Hc]} \right) \quad \text{or} \quad \Delta_{Tr,Hc} = \frac{x_{Tr}}{x_{Hc}} \cdot \frac{[Hc]}{[Tr]} \quad (14)$$

From the known fractionation coefficient $\Delta_{Tr,Hc}$ and the mole fraction x_{Hc} of Hc end member (usually unity or close to a constant if there are two or more major end members), the mole fraction of Tr end member can be estimated as

$$x_{Tr} = \Delta_{Tr,Hc} x_{Hc} \frac{[Tr]}{[Hc]} \quad (15)$$

At every time step, the correction of upper and lower metastability constraints for the host Hc and trace Tr end members is done using the previous amount $n^{(x)}$ of the respective end member and an increment, which is calculated according to kinetic rates, Hc mole fraction, and the Tr mole fraction obtained from the corrected (eq 15) Tr fractionation coefficient:

$$\bar{n}_{Hc,t+\Delta t}^{(x)} = n_{Hc,t}^{(x)} + A_{k,t} R_{n,k,t} \Delta t \cdot x_{Hc,t} \quad (16)$$

$$\bar{n}_{Tr,t+\Delta t}^{(x)} = n_{Tr,t}^{(x)} + A_{k,t} R_{n,k,t} \Delta t \cdot x_{Tr,t} \quad \text{where } x_{Tr,t} = \Delta_{TrHc,t} \frac{[Tr]_t}{[Hc]_t} \quad \text{and } x_{Hc,t} = 1 - x_{Tr,t} \quad (17)$$

Equations as (14) and (15) apply to several *Hc* and *Tr* end members in the solid solution phase, if x_{Hc} and $[Hc]$ in eqs (13,14,15) and (17) are re-defined as the sums of *Hc* components.

1.5. The unified uptake kinetics model (UUKM)

As we have shown previously (*Thien et al., 2013; in revision*), the common outcome from the surface entrapment model (SEMO, *Watson, 2004*) and the surface reaction kinetics model (SRKM, *DePaolo, 2011*) is that the fractionation coefficient $\Delta_{Tr,Hc}$ varies between two limits, $\Delta_{Tr,Hc,eq}$ and $\Delta_{Tr,Hc,ads} = F_{Tr} \cdot \Delta_{Tr,Hc,eq}$. The former limit is related to the (hypothetical) aqueous – solid solution equilibrium; the latter limit corresponds to the distribution of adsorbed *Hc* and *Tr* components in equilibrium with the same aqueous solution of constant composition. F_{Tr} is the so-called trace element enrichment/depletion factor.

These limits suggest that SRKM might be considered as an integrated and simplified form of SEMO, which assumes that the progressing precipitation tends to “entrap” the adsorbed layer composition, whereas the sub-surface layer dynamics (diffusivity) drives its composition to become closer to that in the assumed aqueous- solid solution equilibrium. Since the mineral continues to grow, the uptake of trace elements in ‘older’ layers is, in principle, metastable. This irreversible process of enrichment or depletion of the solid with trace element relative to the expected aqueous- solid equilibrium concentration is called *surface entrapment*.

Relatively fast precipitation augments the composition of the newly-grown layer (i.e. buried adsorbed layer) with the *Tr* content greater than expected from $\Delta_{Tr,Hc,eq}$ if *Tr* is hardly compatible with the host mineral structure ($F_{Tr} > 1$), and less than that if *Tr* is favoured by the bulk mineral lattice ($F_{Tr} < 1$). This enrichment or depletion can be counterbalanced by a concurrent partial release of the entrapped *Tr* back to aqueous solution.

Thus, one can assume that the apparent *Tr* sub-surface diffusivity D_s parameter in SEMO is related to the *Tr* backward rate parameter R_b in SRKM, defined through $v_b R_k = v_k R_b$. This assumption leads to the equality $v_k ml = D_s$ and further to the UUKM equation that predicts the effective fractionation coefficient $\Delta_{Tr,Hc}^*$:

$$\Delta_{Tr,Hc}^* = \Delta_{Tr,Hc,eq} \frac{D_s + R_{L,k} ml}{D_s + \frac{R_{L,k} ml}{F_{Tr}}} \quad (18)$$

where the mineral growth rate $R_{L,k}$ (eq 8) is taken in $\text{nm} \cdot \text{s}^{-1}$. The enrichment parameter F_{Tr} can be, in principle, evaluated if both the *Hc-Tr* solid solution thermodynamic model and the

surface complexation model for *Hc* and *Tr* components on the *Hc* surface is available. The D_s parameter is related to surface dynamics, roughness, and reactivity, and can only be assessed in the inverse modelling.

1.6. Uptake in seed-overgrowth solid solution phases

The setup of aqueous – solid solution uptake kinetics upon the host mineral growth, described in Sections 1.4 and 1.5, has a shortcoming that the composition of the overgrowth is mixed or homogenized with that of the initial seed crystals phase (Fig. 4.2.1,A); it also cannot describe various cases of the (epitaxial) growth on surface of a mineral with other structure.

Therefore, it is desirable to have an option to link the specific surface and the kinetic rates for one “overgrowth” phase to the amount or surface of another “seed” or “substrate” phase; the latter may even be inert, or may have its own slow kinetics. This can be achieved with a *phase linkage*, in which the surface area of one “overgrowth” phase k is determined by the surface area of another (“substrate”) phase s (Fig. 4.2.1,B). If the linkage occurs via the surface area, the relationships between the surface area $A_{k,t}$ and the specific surface area $A_{S,k,t}$ become different from the usual ones as e.g. for the “substrate” phase where

$$A_{k,t} = A_{S,k,t} M_{M,k} n_{k,t} \quad (19)$$

However, in the case B (Fig. 1), this relationship holds constant for the “seed” phase:

$$A_s = A_{S,s} M_{M,s} n_s \quad (20)$$

For the “overgrowth” phase,

$$A_{k,t} = A_{S,k,t} (M_{M,k} n_{k,t} + M_{M,s} n_s). \quad (21)$$

In this case, in the specific surface correction (eq 9), the composite particle size, volume and mass are defined as

$$d_p = \frac{6(V_k + V_s)}{\psi_k A_k}; \quad V_p = \frac{1}{6} \pi d_p^3; \quad \text{and} \quad (22)$$

$$A_p = A_k \frac{V_p}{(V_k + V_s)},$$

respectively.

A similar concept of the *metastability chain* can be further used in thermodynamic modeling of adsorption and ion exchange. In this case, the adsorbed layer (solution) must be linked to the surface of the sorbent similar to the case (Fig.4.2.1,B), but it has a limited thickness (total density). So, instead of growth or condensation, there will be a competition between surface species, described by the Langmuir or another adsorption isotherm.

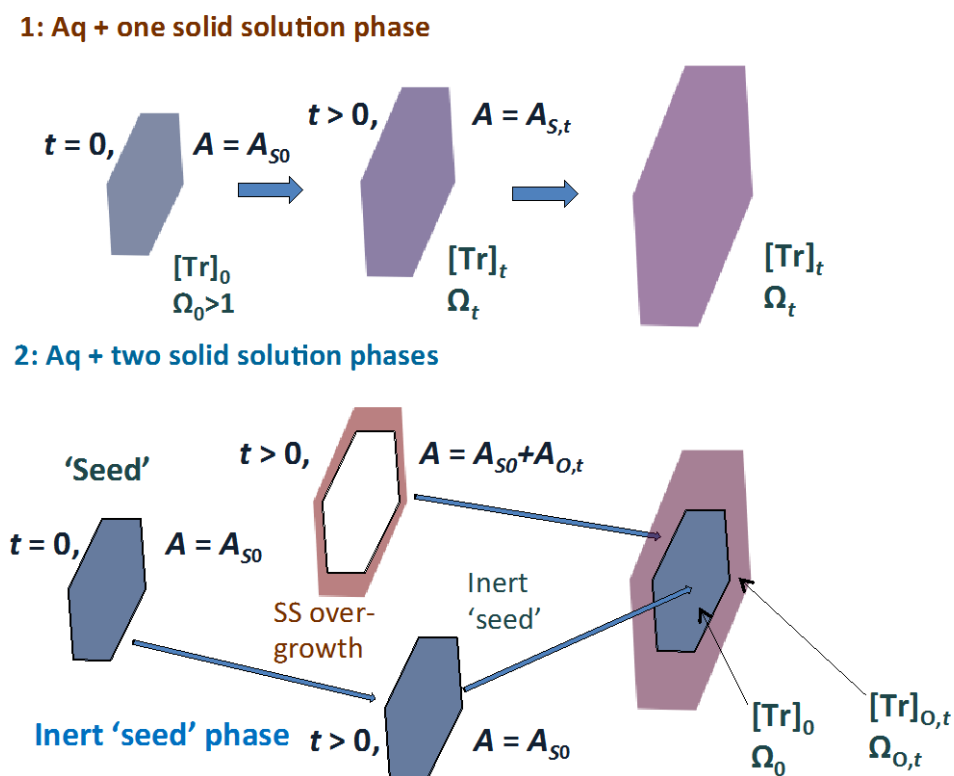


Figure 4.2.1. Schematic representation of two cases of aqueous- solid solution (Aq-SS) uptake: A – single solid solution phase; B – “overgrowth” phase on the surface of “seed” phase, to follow the overgrowth composition independently of the “seed” phase composition.

1.7. Implementation of co-precipitation uptake kinetics in GEMS

Calculations of kinetic rates of mineral-aqueous reactions according to eq (4) have been implemented in the TKinMet class, an extension of the GEMS3K code (*Kulik et al., 2013*), together with the necessary input parameters (Table 4.2.1). GEMS3K can be coupled with mass transport simulation codes to perform reactive transport modelling in an “operator-splitting” fashion (*Shao et al., 2009*).

For each mineral under kinetic rate control, GEMS3K code reads one or more parameter sets for parallel reactions (Table 4.2.1) from the GEM IPM input file, and stores them in a TSolMod class instance. If a positive time step is given, the TSolMod functions are automatically executed after the GEM run, resulting in modified AMRs for the respective mineral phase and its component(s), as given by eqs (1). This process is schematically shown in a flow chart on Fig. 4.2.2.

Table 4.2.1. Input kinetic parameters for *r*-th parallel reaction.

<i>Index</i>	<i>Comment</i>	<i>Symbol</i>	<i>Default value</i>
0	Standard-temperature net rate constant (mol/m ² /s)	$\kappa_{k,r}^+$ or $\kappa_{k,r}^-$	0
1	Standard-temperature gross rate constant (mol/m ² /s)	$K_{k,r}^+$ or $K_{k,r}^-$	0
2	Arrhenius factor	$\Lambda_{k,r}$	1
3	Activation energy (J mol ⁻¹)	$E_{k,r}$	0
4	Empirical parameter related to <i>I</i>	$b_{I,k,r}$	0
5	Empirical parameter related to pH	$b_{pH,k,r}$	0
6	Empirical parameter related to pe	$b_{pe,k,r}$	0
7	Empirical parameter related to Eh	$b_{Eh,k,r}$	0
8	Reaction order parameter for the activity product term	$p_{k,r}$	1
9	Reaction order parameter in the affinity term	$q_{k,r}$	1
10	Parameter in the affinity term	$m_{k,r}$	0
11	Optional constant in the affinity term	$u_{k,r}$	0
12	«Effective» saturation index for nucleation	$\Omega_{k,eff}$	1
13	Second parameter for nucleation (reserved)		0

Notes to Table 4.2.1. If the net rate constant is 0 and gross rate constant is not 0 then the gross rate constant will be used, and vice versa. If both are not 0 then the net rate constant will be used; if both are 0 then this parallel reaction is disabled. The *state of dissolution* of *k*-th phase is detected when $\Omega_k < 1 - \varepsilon_{kin}$; the *state of precipitation* – when $\Omega_k > 1 + \varepsilon_{kin}$; *equilibrium* – when $1 - \varepsilon_{kin} \leq \Omega_k \leq 1 + \varepsilon_{kin}$ ($10^{-8} \leq \varepsilon_{kin} \leq 10^{-4}$ is the numerical tolerance for kinetic calculations). If the net rate constant is positive ($\kappa_{k,r}^+$) and the state is *dissolution* then this parallel reaction will be used, but if the state is *precipitation* then this parallel reaction will be skipped. If the net rate constant is negative ($\kappa_{k,r}^-$) and the state is *precipitation* then this reaction will be used with $|\kappa_{k,r}^-|$, but if the state is *dissolution* then this reaction will be skipped. In a single mineral phase definition, via multiple “parallel reactions”, these rules allow setup of both dissolution and precipitation kinetics, according to different mechanisms, and/or applicable to several aqueous composition regions at varying temperatures.

In this chart, the function KM_Create(*k*) creates a TKinMet instance for *k*-th phase. **GEM IPM**(step) run computes a (partial) equilibrium state in the system at the process step. KM_ParPT(*k*) makes corrections of kinetic and uptake parameters for current T,P. KM_InitTime(*k*) initializes time-dependent values in TkinMet instance; KM_UpdateTime(*k*) updates them for the current time step. KM_UpdateFSA(*k*) updates surface areas and other parameters under external control (e.g. in mass transport); KM_ReturnFSA(*k*) returns such internally changed parameters to external code. KM_InitRates(*k*) initializes kinetic rates and particle/pore properties; KM_CalcRates(*k*) calculates them for the current time step.

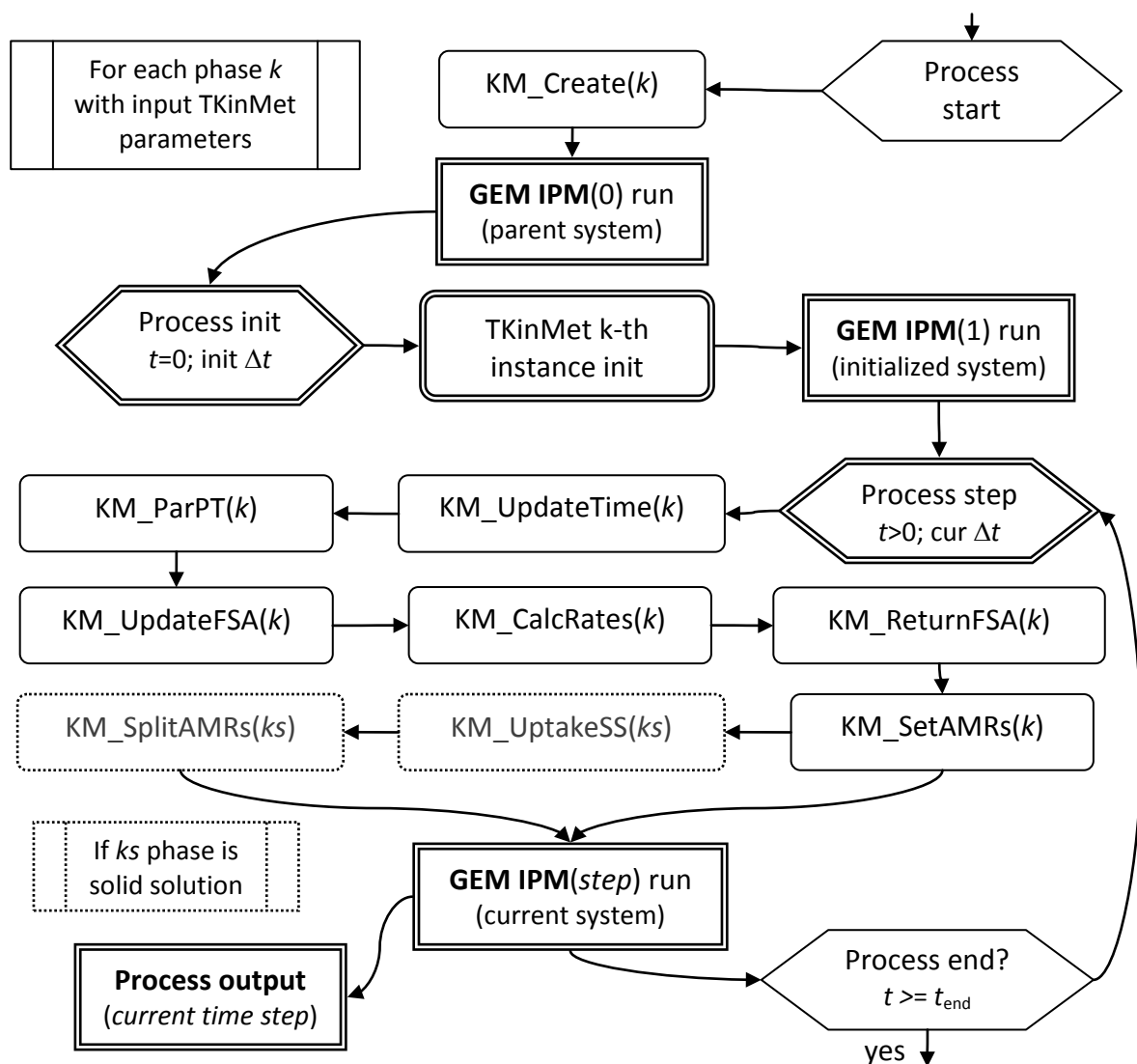


Figure 4.2.2. Flow chart of GEMS process simulation using the TKinMet code library. Three main steps of kinetic simulations are shown: Process start; Process init(ialization); Process run until the end. At each step, TKinMet functions (whose names begin with KM_) are called for each kinetically controlled phase. See text for explanations.

KM_SetAMRs(k) corrects AMRs for k -th phase using current rates and sets them to be used in the next time iteration. Only in the case of uptake in solid solution, KM_UptakeSS(ks) computes new fractionation coefficients and prospective end member mole fractions; then KM_SplitAMRs(ks) uses them to split AMRs for the phase into AMRs for its end members.

The necessary affinity terms (Table 4.2.2) are invoked by choosing the respective code for each parallel reaction.

Preparation of kinetic data is convenient to do using the GEM-Selektor v.3.3 code prototype, where such phase definitions with all necessary coefficients can be saved as Phase records in the modeling project database. Selection of aqueous, gaseous, or surface species for the activity product term (eq 7) is also stored in the Phase definition as a list of DComp or ReacDC record keys with respective reaction stoichiometry power coefficients $b_{j,k,r}$.

Table 4.2.2. Selection of affinity terms currently implemented in the TKinMet library

Code	Expression	Comment, reference
0	$(1 + u_{k,r} - \Omega_k^{q_{k,r}})^{m_{k,r}}$	Normal (default) affinity term
1	$(\Omega_k^{q_{k,r}} - 1 - u_{k,r})^{m_{k,r}}$	Inverse normal affinity term
2	$e^{-m_{k,r}/\Omega_k}$	(Schott et al., 2012), Fig. 1e
3	$1 - e^{-(q_{k,r} \ln \Omega_k)^{m_{k,r}}}$	(Hellmann and Tisserand, 2006), eq 9
4	$m_{k,r}(\Omega_k - 1) \cdot \ln \Omega_k$	(Teng et al., 2000), eq 13
5	$\Omega_k^{m_{k,r}}$	Nucleation (Teng et al., 2000), Fig. 6
6	$(\Omega_k - \Omega_{k,eff})^{m_{k,r}}$	Nucleation and growth (Fritz et al., 2009), eq 6

Notes to Table 4.2.2. $\Omega_{k,eff} \geq 1$ is the effective saturation index (default value 1) at the onset of nucleation. More choices of affinity terms will possibly be added in order to accommodate the rate laws available in literature for mineral-aqueous reactions.

Parameters of the uptake kinetics model described in section 1.5 and listed in Table 4.2.3 are supplied only in the solid solution Phase definition record in addition to the parameters for mineral-water reaction kinetics. The value of $\Delta_{Tr,Hc,eq}$ can be found in preliminary GEM calculations of aqueous-solid solution equilibria, or taken from the literature. Other parameters in Table 4.2.3 should be estimated as described in WP4 Task 1 mid-term report.

If the metastability linkage between the “overgrowth” solid solution and the “substrate” phase needs to be considered (section 1.6), it has to be provided as a special option in the Phase record for the “overgrowth” phase. There the record key of the “substrate” phase is selected from the modeling project database, along with the type and parameters for the linkage. Currently, the link to the “substrate” phase surface area is implemented, with a parameter being an effective fraction of surface to be used in scaling the amount of overgrowth phase over time steps (default fraction is unity).

Table 4.2.3. *Uptake model parameters*

<i>Index</i>	<i>Comment</i>	<i>Symbol</i>	<i>Default</i>
0	Surface enrichment/depletion factor	F_{Tr}	1
1	Tr fractionation coefficient in solid solution in equilibrium with the medium	$\Delta_{Tr,Hc,eq}=\alpha_{eq}$	1
2	Tr surface diffusivity, nm^2s^{-1}	D_s	0
3	lattice diffusion coefficient, nm^2s^{-1}	D_l	0
4	half-thickness of surface enriched/depleted layer (nm)	l	0
5	multiplier linking l to the maximal thickness of the diffusivity region	m	1

The whole simulation of kinetically-dependent system can be performed in the Process Simulator mode of GEM-Selektor v.3.3 package prototype. The TKinMet calculations are automatically activated when the time iterator of the process is set with the positive time step value and more than one step.

Technical details can be found in Phase and Process create/remake wizards, as well as in the GEM-Selektor runtime help database. Note that in the provided software, the TKinMet library options have been tested only for the methods described above and using only the test systems described in Section 2 below. Before the general use of the software becomes possible, many more extensions, tests and benchmarks need to be performed in on-going and future projects.

2. Modelling examples and verification

The idea of simulation examples was to test and verify the new functionality implemented in the TKinMet code library of GEMS3K code, as well as Phase and Process simulator modules of GEM-Selektor code. The test example about portlandite shows how the seeded mineral growth is simulated, and why the proper shape factor function for the A_S correction may be needed to fit the experimental data. The example for calcite precipitation verifies the growth rate model (*Wolthers et al., 2012*) against the independent experimental data. This rate model for calcite is used as a background in other test simulations, aimed at showing how the UUKM (eq 18) describes the strontium uptake upon calcite growth, with important effects such as the impact of growth-rate variation and/or solution depletion.

2.1. Seeded growth of portlandite

This example shows a simulation of seeded precipitation of portlandite $\text{Ca}(\text{OH})_2$ from aqueous solution at room temperature, with kinetic rate constant and shape factor function parameterized against the experimental data (*Tadros et al., 1976*). In these experiments, the

supersaturated solutions were prepared by mixing equal volumes of 0.07 M CaCl₂ and 0.14 M NaOH stock solutions under CO₂-free conditions. In one series of experiments, the crystallization of portlandite was initiated by adding 10 mg of seed crystals with specific surface area $A_S = 2.1 \text{ m}^2 \cdot \text{g}^{-1}$ to 300 ml of the supersaturated solution. The time variation of the conductance was followed until constant readings achieved in about 90 min. Plots of $\log(\text{conductance at } t - \text{conductance at equilibrium})$ were assumed proportional to $\log([\text{Ca}]_{\text{aq},t} - [\text{Ca}]_{\text{aq,eq}})$, provided that the Cl⁻ and Na⁺ concentrations remain constant during growth. Using this assumption, initial $[\text{Ca}]_{\text{aq}} = 0.0351 \text{ m}$, and equilibrium $[\text{Ca}]_{\text{aq,eq}} = 0.0231 \text{ m}$ (Table 4.2.4), we have converted in a spreadsheet the conductance data (Fig. 2 in *Tadros et al., 1976*) into total dissolved $[\text{Ca}]_{\text{aq}}$ values, with the estimated uncertainty less than $0.3 \cdot 10^{-3} \text{ m}$.

Table 4.2.4. Initial recipe of the chemical system “PortlKinExp” for the Process simulation

<i>Property</i>	<i>Name</i>	<i>Quantity</i>	<i>Units</i>	<i>Comment</i>
xa_	Aqua (H ₂ O)	299.26	g	Addition of 300 ml water H ₂ O at 1 bar, 25 C
xa_	CaCl ₂	0.0105	mol	Addition of 0.0105 moles of CaCl ₂ (in 150 ml of 0.07 M CaCl ₂ solution)
xa_	NaOH	0.021	mol	Addition of 0.021 moles of NaOH (in 150 ml of 0.14 M NaOH solution)
xd_	Portlandite	0.01	g	Addition of 10 mg Ca(OH) ₂ “seed” crystals
bi_	Nit	0.0016	mol	Addition of atmospheric nitrogen
bi_	O	0.0004	mol	Addition of oxygen (to form a CO ₂ -free atmosphere)
dul_	Portlandite	0.000135	mol	Upper AMR for 10 mg of “seed” portlandite

“Property” identifies an entry in the GEM-Selektor Recipe dialog.

Model calculations have been performed using the GEM-Selektor v.3.3 code prototype, in the “Kinetics” test modeling project, at $P = 1 \text{ bar}$, $T = 25 \text{ C}$. The initial system recipe was set as given in Table 4.2.4; the Davies equation was used for computing aqueous activity coefficients. The input thermodynamic data were taken from GEMS version of the PSI-Nagra database 01/07 (*Thoenen, 2012*; <http://gems.web.psi.ch/TDB>). The GEM-calculated initial saturation index of portlandite was 2.836, the total dissolved $[\text{Ca}]_{\text{aq}} = 0.0351 \text{ m}$. In a separate GEM calculation of equilibrium in the same system without the upper AMR for portlandite, $[\text{Ca}]_{\text{aq,eq}}$ was found to be equal to 0.0231 m .

Kinetic parameters of the Portlandite phase were set according to a simple rate equation $R_{\text{Port}} = \kappa_{\text{Port}}^- (1 - \Omega_{\text{Port}})$. The rate constant value κ_{Port}^- together with the dependence of the sphericity factor ψ_{Port} on saturation index given as $\psi_{\text{Port}}(t) = \psi_0 + \psi_1 u$ where $u = \log_{10} \Omega_{\text{Port},t}$, were adjusted in trial-and-error process simulations using the CEM-Selektor Process module with Graphics dialog.

The time interval was [0; 6000] s with time step Δt of 15 or 30 s; no visible differences on the model curves were found with these Δt values. Excellent fit to the experimental conductivity data (Fig. 4.2.3) was obtained with parameters given in Table 4.2.5.

Table 4.2.5. Parameters of the kinetic model for portlandite seeded growth.

Parameter	Value	Comment
Net rate constant at 25 C κ_{Port}^- (mol·m ⁻² ·s ⁻¹)	-3.23·10 ⁻⁵	Fit to data
Arrhenius factor Λ_{Port}	1.0	Default
Activation energy E_{Port}	0	Default
Reactive surface area fraction θ_{Port}	1.0	Default
Sphericity factor dependence $\psi_0 + \psi_1 u$: ψ_0	0.83	Geometry;
ψ_1	-1.6	fit to data
Initial specific surface area $A_{S,Port,0}$ (m ² ·g ⁻¹)	2.1	experiment
Initial portlandite “seed” mass m_{Port} (g)	0.01	experiment

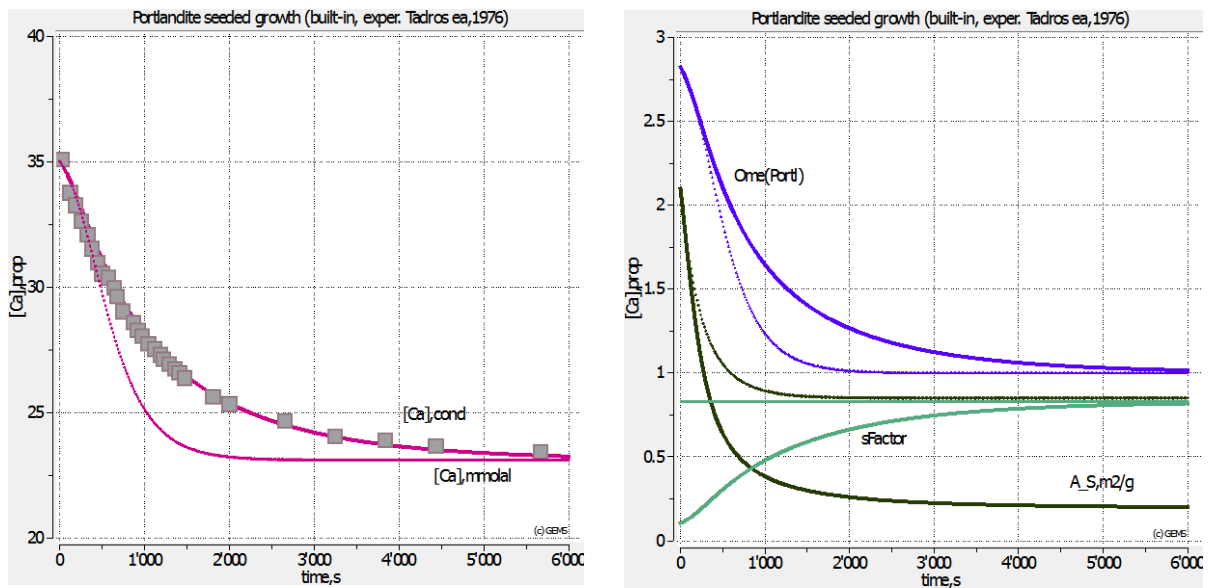


Figure 4.2.3. Simulation of seeded growth of portlandite (dense curves) in comparison with experimental data from (Tadros et al., 1976) (squares) and another simulation with constant sFactor (sphericity factor) $\psi_{Port} = 0.83$ (thin dotted curves). $Ome(Portl)$ denotes $\Omega_{Port,t}$.

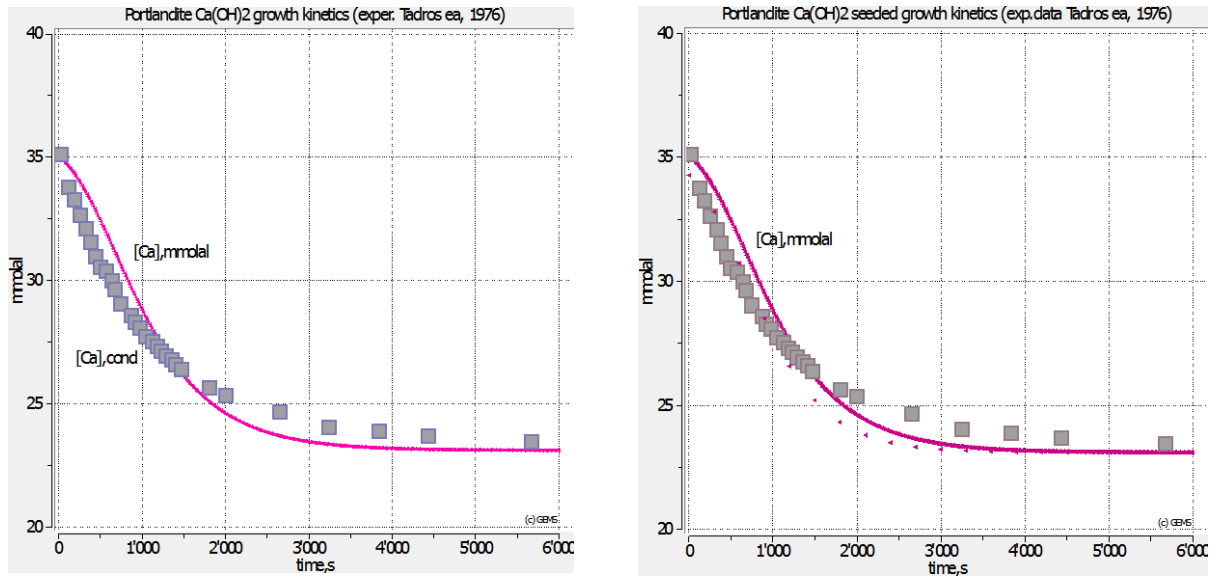


Figure 4.2.4. Sensitivity of kinetic simulations of seeded growth of portlandite. Left-hand side: “best fit” with $\psi_{port} = 1.0$, $\kappa_{port}^- = -2.1 \text{ mol}\cdot\text{m}^{-2}\cdot\text{s}^{-1}$, and $\Delta t = 15$ or 30 s. Right-hand side: the same model run compared with the one at time stepping of $\Delta t = 300$ s (dots).

For comparison, Fig. 4.2.3 shows curves simulated with the same parameters, but without the correction of shape factor (sphericity), kept constant at its “equilibrium” value of 0.83. This shows that a significant change in morphology of portlandite particles must take place during the early stages of growth. This is indirectly corroborated by (Tomazic *et al.* 1986) who provide the evidence of morphology changes upon portlandite precipitation.

Some other model sensitivity cases are given in Fig. 4.2.4, on the left-hand side of which the “best” fit at constant $\psi_{port} = 1.0$ and $\kappa_{port}^- = -2.1 \text{ mol}\cdot\text{m}^{-2}\cdot\text{s}^{-1}$ shows that the absence of shape factor correction results in a wrong shape of the model curve that cannot be fixed by adjusting the rate constant. The right-hand side shows the impact of too large time step duration Δt . To find the optimal time stepping is a non-trivial issue, which requires more investigation. Presently, the practical rule would be to demonstrate that the same model curve is produced with two different (small enough) time step length values.

2.2. Calcite precipitation

For modelling kinetics of trace element uptake in calcite, eq (18) must be combined with the calcite precipitation rate law. We used the rate law (at $T = 20$ C) from (Wolthers *et al.*, 2012):

$$R_{L,Cal} = I^{-0.004} pH^{-10.71} \cdot \left(\frac{a_{Ca^{2+}}}{a_{CO_3^{2-}}} \right)^{-0.35} \cdot (\Omega^{0.5} - 1)^2 \quad (23)$$

where $R_{L,Cal}$ is the mean orthogonal surface propagation velocity (in $\text{m}\cdot\text{s}^{-1}$). It can be converted using eq (8) into the net precipitation rate R_{Cal} (in $\text{mol}\cdot\text{m}^{-2}\cdot\text{s}^{-1}$):

$$R_{Cal} = 10^6 \frac{R_{L,Cal}}{V_{M,Cal}} = 27075.3 \cdot R_{L,Cal} \quad (24)$$

where $V_{M,cal} = 36.934 \text{ cm}^3\cdot\text{mol}^{-1}$ is the calcite molar volume. For seawater (diluted and undiluted), **Wolthers et al. (2012)** proposed a slightly different rate law to account for the inhibition effects of Mg^{2+} and other ions:

$$R_{L,Cal,SW} = I^{0.36} pH^{-10.99} \cdot \left(\frac{a_{Ca^{2+}}}{a_{CO_3^{2-}}} \right)^{-0.71} \cdot (\Omega^{0.5} - 2)^2 \quad (25)$$

The activation energy of calcite is $48.1 \text{ kJ}\cdot\text{mol}^{-1}$ at $T = 25 \text{ C}$ (**Inkseep and Bloom, 1985**).

Using eq (6) yields the Arrhenius constant $\Lambda_{k,r} = 1 \cdot e^{\frac{-E_{k,r}^\ddagger}{R \cdot 298.15}} = 2.6706 \cdot 10^8$ leading to the temperature correction factor from 298 to 293 K equal to 0.7163. Coefficient $-27075.3/0.7163 = -37800$ can now be put for the rate constant κ_{Cal}^- used in TKinMet “standard” form eq (4).

Let us check the rate equation (23) on an example for seeded precipitation of calcite CaCO_3 from aqueous solution at $T = 10 \text{ C}$, compared with the experimental data (**Dreybrodt et al. 1997**). These authors prepared supersaturated solutions by dissolving CaCO_3 powder and CO_2 in deionized water. Immediately after filling the vessel with the supersaturated solution ($4 \cdot 10^{-3} \text{ M}$ $[\text{Ca}^{2+}]$), 3.16 mmol of calcite seed (with $A_{S,0} = 0.184 \text{ m}^2\cdot\text{g}^{-1}$) was introduced. Because of calcite precipitation, $[\text{Ca}^{2+}]_t$ (monitored by conductance measurements) decreased with time tending toward the equilibrium $[\text{Ca}^{2+}]_{\text{eq}}$ value of $2.8 \cdot 10^{-3} \text{ M}$.

Simulations at 1 bar, 10°C were performed in the “Kinetics” test modeling project using the GEM-Selektor v.3.3 prototype. The Davies equation was used for computing aqueous activity coefficients. Thermodynamic data were taken from the GEMS version of the PSI-Nagra database 01/07 (**Thoenen, 2012**; <http://gems.web.psi.ch/TDB>). The initial system recipe is given in Table 4.2.6. The GEM calculation for this system yields the initial saturation index of calcite ($\log_{10}\Omega_{Cal} = 2.53$). Note that this system is extremely sensitive to the addition of CO_2 to bulk composition. The value in Table 4.2.6 was found by trial-and-error to set calculated $p\text{CO}_2 = 0.001 \text{ bar}$, as mentioned by **Dreybrodt et al. (1997)**.

Kinetic parameters in the Calcite phase record were set according to Table 4.2.7. The sphericity factor of calcite was set constant at $\psi_{Cal} = 0.8$. Process simulations were performed in the time interval $[0; 44000] \text{ s}$ with the time step $\Delta t = 10 \text{ s}$ (Fig. 4.2.5).

The model reproduces well the measured $[\text{Ca}^{2+}]$ at times longer than 8000 s. Some deviation at shorter times may be due the “seed” sample heterogeneity or variation in particle morphology upon growth, both not accounted for in the present model. In general, a good fit

to the experimental data without any parameter adjustment confirms the validity of calcite growth kinetic rate equation (*Wolthers et al., 2012*), especially at close-to-equilibrium conditions and slow rates.

Table 4.2.6. Initial recipe of the chemical system “Calcite” for the GEM process simulation

Property	Name	Quantity	Units	Comment
xa_	Aqua	262	g	Addition of 262 ml water H ₂ O at 1 bar, 10°C
xa_	CaCO ₃	0.00435	mol	Addition of 0.00435 moles of CaCO ₃ for both the solution and the seed calcite.
xa_	CO ₂	0.0011	mol	Addition of 0.011 moles of CO ₂ to obtain pCO ₂ = 1·10 ⁻³ bar (adjusted by trial-end-error)
xa_	O ₂	1·10 ⁻⁶	mol	Addition of O ₂ to stabilize redox state
dll_	Calcite	0.00316	mol	Lower AMR for 0.00316 mol of “seed” calcite
dul_	Calcite	0.00316	mol	Upper AMR for 0.00316 mol of “seed” calcite

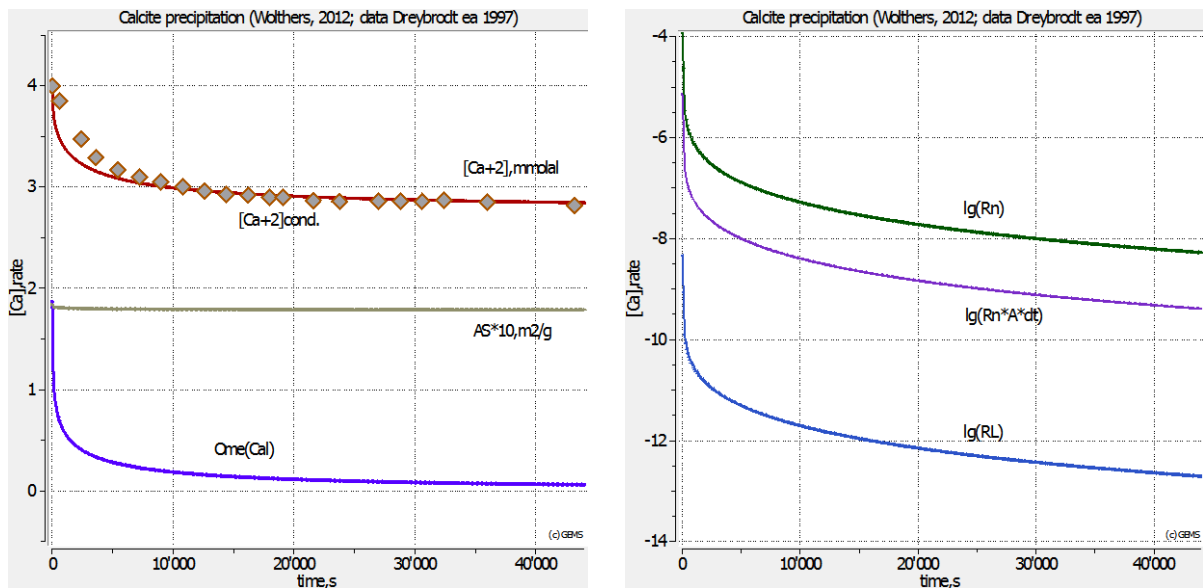


Figure 4.2.5. Simulations of calcite precipitation with kinetic parameters from Table 4.2.7. Calcite specific surface area $AS \cdot 10$ is $10 \cdot A_{S,cal}$ in $m^2 \cdot g^{-1}$. $Ome(Cal)$ is the current stability index Ω_{Cal} of calcite. Decimal logarithmic rates (right-hand side) are shown in $mol \cdot m^{-2} \cdot s^{-1}$ (Rn); in moles per time step ($Rn \cdot A \cdot dt$); and in $m \cdot s^{-1}$ (RL).

2.3. Simulations of Sr and Cd uptake kinetics in calcite

In this example for seeded co-precipitation of the “incompatible” cation Sr^{2+} in calcite CaCO_3 from aqueous solution, the uptake kinetics model has been parameterized against the experimental data by (*Lorens 1981*). In this experiment, the precipitation of calcite was triggered by a constant addition of Na_2CO_3 stock solution with a rate $2.16 \cdot 10^{-8} \text{ mol} \cdot \text{s}^{-1}$ to the initial solution, which induced an average calcite growth rate of $2.94 \cdot 10^{-6} \text{ mol} \cdot \text{m}^{-2} \cdot \text{s}^{-1}$.

Simulations have been performed using the GEM-Selektor v.3.3 code prototype, in the “LorensSrCa” test-modeling project, at 1 bar, 25°C. The initial system recipe is given in Table 4.2.8; the Extended Debye-Hückel equation was used for aqueous activity coefficients. The input thermodynamic data were taken from the GEMS version of PSI-Nagra database 01/07.

A solid-solution phase Calcite-Sr_ovg consisted of two end-members, Cal (calcite) and $\text{SrCO}_3\text{-cal}$ (SrCO_3 with calcite structure), and a regular parameter $W_G = 4.4 \text{ kJ} \cdot \text{mol}^{-1}$ (*Kulik et al. 2010*). This phase was initially used without AMRs to calculate the equilibrium fractionation coefficient $\Delta_{\text{Sr,Ca,eq}} = 0.021$. The recipe of the initial system is provided in Table 4.2.8. Kinetic rate parameters for the Calcite-Sr_ovg phase were taken the same as in Table 4.2.7; the UUKM parameters were set according to Table 4.2.9. The Calcite-Sr_ovg phase was linked to the surface area of the Calcite_seed pure phase, with the initial $A_{\text{S,Cal}} = 0.8 \text{ m}^2 \cdot \text{g}^{-1}$.

Table 4.2.8. Recipe of initial chemical system “SrCaLorens7” for the Process simulation

Property	Name	Quantity	Units	Comment
xa_	Aqua	150	g	Addition of 150 ml water H_2O at 1 bar, 25°C
xa_	NaCl	0.1035	mol	Addition of 0.1035 moles of NaCl
xd_	NaHCO_3	0.00145	mol	Addition of 0.00145 moles of NaHCO_3
xa_	CaCl_2	0.0015	mol	Addition of 0.0015 moles of CaCl_2
xa_	Na_2CO_3	$1 \cdot 10^{-7}$	mol	Addition of $1 \cdot 10^{-7}$ moles of Na_2CO_3
xa_	CaCO_3	$9.2 \cdot 10^{-5}$	mol	Addition of $9.2 \cdot 10^{-5}$ moles of CaCO_3 for seed
xd_	Sr+2	$4.59 \cdot 10^{-8}$	mol	Addition of $4.59 \cdot 10^{-8}$ moles of SrCl_2
xd_	Cl-	$9.18 \cdot 10^{-8}$	mol	Addition of $4.59 \cdot 10^{-8}$ moles of SrCl_2
xa_	CO_2	0.055	g	Addition of CO_2 to equilibrate the solution
xa_	O_2	0.1	g	Addition of O_2 to set redox state
xa_	N_2	3	g	Addition of N_2 to equilibrate the solution
dll_	Cal_seed	$9.2 \cdot 10^{-5}$	mol	Lower AMR set for “seed” calcite
dul_	Cal_seed	$9.2 \cdot 10^{-5}$	mol	Upper AMR set for “seed” calcite

Process simulation: titration by adding Na_2CO_3 with a rate $2.16 \cdot 10^{-8} \text{ mol} \cdot \text{s}^{-1}$.

A first Process simulation has been run within the time interval [0; 540] s (actual duration of the experiment) with time step of 1 s. To explore the potential depletion effects, the second simulation has been performed within a hypothetical longer time interval [0; 10000] s. The results are shown in Fig. 4.2.6. They indicate a similar enrichment of Sr in over-grown calcite as in the experiments (*Lorens, 1981*), whereas at long reaction time, the aqueous solution depletion effect drives the effective Sr fractionation coefficient back to its aqueous-solid solution equilibrium value (0.021) and then to much lower values.

Table 4.2.9. Parameters of the uptake kinetic model for Sr in calcite

<i>Comment</i>	<i>Value</i>	<i>Reference</i>
Initial specific surface area $A_{S,0}$ ($\text{m}^2 \cdot \text{g}^{-1}$)	0.8	experiment
Initial calcite “seed” mass (g)	$9.2 \cdot 10^{-3}$	experiment
Surface enrichment factor F_{Sr}	6.2	(<i>Thien et al., 2013</i>)
Equilibrium fractionation coefficient $\Delta_{Sr,Ca,eq}$	0.021	(<i>Kulik et al., 2010</i>)
Sr sub-surface diffusivity $D_{s,Sr}$ ($\text{nm}^2 \cdot \text{s}^{-1}$)	0.02	(<i>Thien et al., 2013</i>)
Sr lattice diffusivity in calcite $D_{l,Sr}$ ($\text{nm}^2 \cdot \text{s}^{-1}$)	$1 \cdot 10^{-16}$	the same
Length l at which DS applies in the subsurface layer (nm)	0.5	the same
Length multiplier m	6	the same

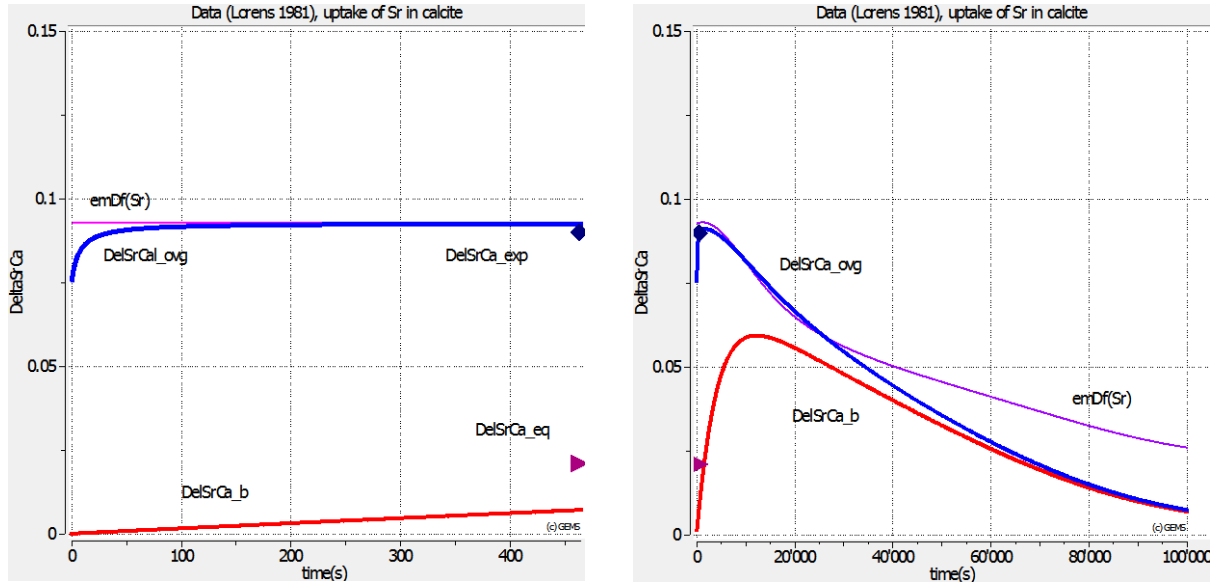


Figure 4.2.6. Simulations of time-dependent uptake of Sr in calcite (different time scales on left- and right-hand sides). $\text{DelSrCa}_{\text{exp}}$: experimental $\Delta_{Sr,Ca}$; $\text{DelSrCa}_{\text{eq}}$: aqueous – solid solution equilibrium $\Delta_{Sr,Ca,eq}$; $\text{emDf}(Sr)$: effective $\Delta_{Sr,Ca}$ (eq 18); $\text{DelSrCa}_{\text{ovg}}$: average $\Delta_{Sr,Ca}$ in the overgrowth phase; $\text{DelSrCa}_{\text{b}}$: bulk $\Delta_{Sr,Ca,eq}$ in the seed + overgrowth phase.

In another example, the seeded precipitation of “compatible element” cadmium with calcite at 1 bar, 25 C has been simulated and compared with the experimental data (*Lorens, 1981*). As in the previous example, the process is driven by constant addition of Na₂CO₃ at the rate $8.37 \cdot 10^{-9} \text{ mol} \cdot \text{s}^{-1}$ that induces the initial growth rate of calcite $R_{n,Cal} = 2.975 \cdot 10^{-6} \text{ mol} \cdot \text{m}^{-2} \cdot \text{s}^{-1}$.

Simulations have been performed in the “CdCalcite” test modeling project. The initial system recipe was set as given in Table 4.2.10; the Extended Debye-Hückel equation was used for computing aqueous activity coefficients. The input thermodynamic data were from the GEMS version of the PSI-Nagra database 01/07; those for otavite CdCO₃ - from (*Gamsjäger et al., 1999*); and for Cd aqueous species – from the SUPCRT database (built-in in GEM-Selektor).

A solid-solution Calcite-Ota_ovg consists of two end-members, Cal (calcite) and Otavite (CdCO₃), with the regular interaction parameter $W_G = 2.975 \text{ kJ mol}^{-1}$ (*Tesoriero and Pankow, 1996*). This phase was initially used without AMRs to calculate the equilibrium fractionation coefficient $\Delta_{Cd,Ca,eq} = 33.0$; the recipe of the initial system is provided in Table 4.2.10. Kinetic rate parameters for the Calcite-Ota_ovg phase were taken the same as in Table 4.2.7; the UUKM parameters were set according to Table 4.2.11. The Calcite-Ota_ovg phase was linked to the surface area of the Calcite_seed pure phase, with initial $A_{S,Cal} = 0.8 \text{ m}^2 \cdot \text{g}^{-1}$.

Table 4.2.10. Recipe of initial chemical system “CdCaLorens2” for the Process simulation

<i>Property</i>	<i>Name</i>	<i>Quantity</i>	<i>Units</i>	<i>Comment</i>
xa_	Aqua	150	g	Addition of 150 ml water H ₂ O at 1 bar, 25°C
xa_	NaCl	0.1035	mol	Addition of 0.1035 moles of NaCl
xd_	NaHCO ₃	0.0017	mol	Addition of 0.0017 moles of NaHCO ₃
xa_	CaCl ₂	0.0015	mol	Addition of 0.0015 moles of CaCl ₂
xa_	CaCO ₃	$3.1 \cdot 10^{-5}$	mol	Addition of $3.1 \cdot 10^{-5}$ moles of CaCO ₃ for seed
xd_	Cd+2	$1 \cdot 10^{-6}$	mol	Addition of $1 \cdot 10^{-6}$ moles of CdCl ₂
xd_	Cl-	$2 \cdot 10^{-6}$	mol	Addition of $1 \cdot 10^{-6}$ moles of CdCl ₂
xa_	CO ₂	0.043	g	Addition of CO ₂ to equilibrate the solution
xa_	O ₂	0.1	g	Addition of O ₂ to equilibrate the solution
xa_	N ₂	2	g	Addition of N ₂ to equilibrate the solution
dll_	Cal_Seed	$3.1 \cdot 10^{-5}$	mol	Lower AMR for $3.1 \cdot 10^{-3}$ g of “seed” calcite
dul_	Cal_Seed	$3.1 \cdot 10^{-5}$	mol	Upper AMR for $3.1 \cdot 10^{-3}$ g of “seed” calcite
dul_	Cal	$1 \cdot 10^{-10}$	mol	Upper AMR for $1 \cdot 10^{-10}$ mol of calcite end member
dul_	Otavite	$1 \cdot 10^{-12}$	mol	Upper AMR for $1 \cdot 10^{-12}$ mol of otavite end member

The first Process simulation has been run in the time interval [0; 1200] s (actual duration of the experiment) with time step of 10 s. To explore the potential aqueous solution depletion

effects, the second simulation has been run within a longer time interval [0; 100000] s with time step of 100 s. The results are shown in Fig. 4.2.7. They indicate the same depletion of Cd in over-grown calcite as observed in the experiments (*Lorens, 1981*), whereas at long reaction times, the aqueous solution depletion effect would drive the effective Cd fractionation coefficient up to its aqueous-solid solution equilibrium value.

Table 4.2.11. Parameters of the uptake kinetic model for Cd in calcite

Comment	Value	Reference
Initial specific surface area $A_{s,0}$ ($\text{m}^2 \cdot \text{g}^{-1}$)	0.8	experiment
Initial calcite “seed” mass (g)	$3.1 \cdot 10^{-3}$	experiment
Surface enrichment factor F_{Cd}	0.3	(<i>Thien et al., 2013</i>)
Equilibrium fractionation coefficient $\Delta_{Cd,Ca,eq}$	33.0	(<i>Tesoriero and Pankow, 1996</i>)
Cd sub-surface diffusivity $D_{s,Cd}$ ($\text{nm}^2 \cdot \text{s}^{-1}$)	0.02	(<i>Thien et al., 2013</i>)
Cd lattice diffusivity in calcite $D_{l,Cd}$ ($\text{nm}^2 \cdot \text{s}^{-1}$)	$1 \cdot 10^{-16}$	the same
Length l at which D_s applies in the subsurface layer (nm)	0.5	the same
Length multiplier m	6	the same

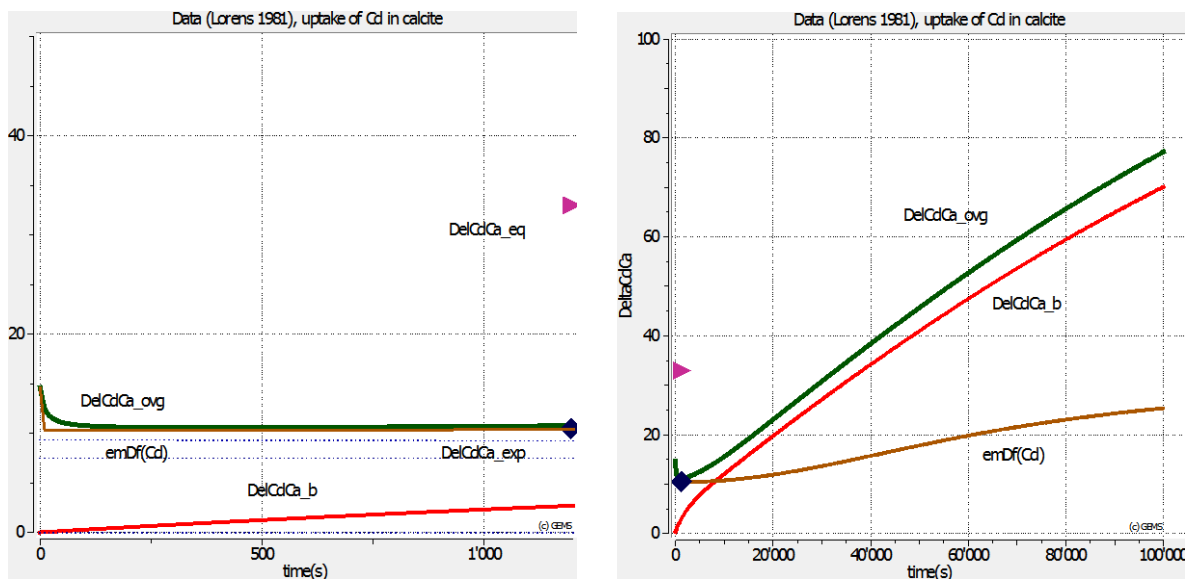


Figure 4.2.7. Simulations of time-dependent uptake of Cd in calcite (different time scales on left- and right-hand sides). $\Delta_{Cd,Ca,exp}$: experimental $\Delta_{Cd,Ca}$; $\Delta_{Cd,Ca,eq}$: aqueous – solid solution equilibrium $\Delta_{Cd,Ca,eq}$; $emDf(Cd)$: effective $\Delta_{Cd,Ca}$ (eq 18); $\Delta_{Cd,Ca,ovg}$: average $\Delta_{Cd,Ca}$ in the overgrowth phase; $\Delta_{Sr,Ca,eq}$ in the seed + overgrowth phase.

2.4. Simulation of Sr uptake in calcite from the seawater –air system

The idea of this example was to demonstrate the potentially complex uptake processes on the background of temperature, composition change, and depletion effects in aqueous- solid solution systems that can be modeled with the new TKinMet code functionality. The obtained predictions may comprise a challenge for future experimental verifications. We also compare both one- and two- solid solution cases as outlined in Fig. 4.2.1.

One solid solution case. The initial chemical system “Sr-calcite” was set in the “CarbSea” test modeling project, using the recipe in Table 4.2.8 and the Extended Debye-Hückel equation with the common size parameter for aqueous activity coefficients. The input thermodynamic data was taken from the GEMS version of the PSI-Nagra database 01/07.

The solid-solution phase Calcite-Sr_ovg with two end-members, Cal (calcite) and SrCO3-cal (SrCO₃ with calcite structure), and a regular parameter $W_G = 4.4 \text{ kJ}\cdot\text{mol}^{-1}$ was included into the system definition. This phase model is the same as that considered in Section 2.3 above. Kinetic rate parameters for the Calcite-Sr_ovg phase were taken the same as in Table 4.2.7; the UUKM parameters were set as in Table 4.2.12, except that initial $A_{S,0}$ set equal to $0.09 \text{ m}^2\cdot\text{g}^{-1}$. In Fig. 4.2.8, the results of simulations at $P = 1 \text{ bar}$, $T = 25 \text{ C}$ and 15 C are presented.

Table 4.2.12. Recipe of initial chemical system “SrCalcite” for the Process simulation

Property	Name	Quantity	Units	Comment
xa_	Aqua	965	g	Addition of H ₂ O to produce 1 kg of seawater
xa_	AtmAirNit	10	kg	Atmosphere (pCO ₂ = 36 Pa)
xa_	CaCO ₃	$1.0\cdot 10^{-4}$	mol	Addition of 0.1 mmoles of CaCO ₃ for seed
xd_	SeaSalt	35	g	Addition of 35 g normative sea salt
dul_	Cal	$1.001\cdot 10^{-4}$	mol	Upper AMR set for $10 \text{ mg}\cdot\text{kgw}^{-1}$ “seed” calcite
dul_	SrCO3-cal	$1.8\cdot 10^{-10}$	mol	Upper AMR set for trace Sr content in “seed” calcite

Process simulation: titration by adding Na₂CO₃ with a rate of 0.05 mmol per hour; time interval: [0; 200] h; time step $\Delta t = 1 \text{ h}$. Normative sea salt composition (in mmol·kgw⁻¹, without H₂O):

C	1.93895	Mg	54.9493
Ca	10.6366	Na	484.336
Cl	565.497	O	123.597
H	2.339	S	29.1959
K	10.5568	Sr	0.09308

The linked two-solid-solutions case. The initial chemical system “Sr-calc-ovg” was set in the “CarbSea” test modeling project, using the recipe in Table 4.2.8 and other features similar to the previous case. Two solid solution phases were included. The “seed” ArgStr phase with end members Arg (aragonite) and Str (strontianite) had the properties from (*Kulik et al., 2010*);

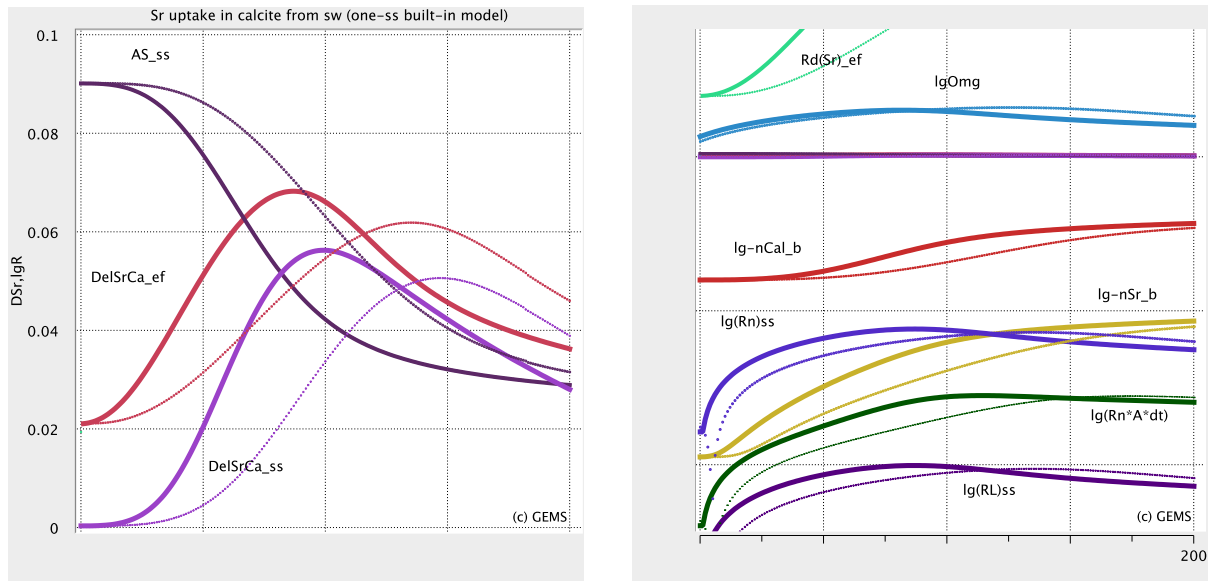


Figure 4.2.8. Simulation runs for one-phase case of Sr uptake in calcite from seawater, showing the effects of temperature (thick curves: $T=25$ C, thin dotted curves: $T=15$ C), varying precipitation rate, and seawater depletion. $DelSrCa_{ef}$: effective $\Delta_{Sr,Ca}$ (eq 18); $DelSrCa_{ss}$: bulk $\Delta_{Sr,Ca}$ in solid solution phase; AS_{ss} : specific surface area; $lgOmg$: saturation index; $nCal_b$ and nSr_b : amounts of end members; Rn , RL and $Rn \cdot A \cdot dt$: precipitation rates in $\text{mol} \cdot \text{m}^{-2} \cdot \text{s}^{-1}$, $\text{m} \cdot \text{s}^{-1}$, and mol per time step, respectively.

the amount of Arg was fixed by lower and upper AMRs at 0.0001 mol, and the amount of Str end member fixed at 10^{-9} mol; the initial specific surface area was $A_{S,0} = 0.09 \text{ m}^2 \cdot \text{g}^{-1}$. The “overgrowth” solid-solution phase Calcite-Sr_ovg with end-members, Cal (calcite) and SrCO₃-cal (SrCO₃ with calcite structure) was the same as in the previous case, except that it was linked to the surface of the “seed” phase. The time step and interval were the same as before.

The simulation results for this case are shown in Fig. 4.2.9, where the variation of the amount and composition of the “overgrowth” phase can now be followed separately from the “seed” phase. Variation of the “bulk solid” Sr fractionation coefficient is clearly the same as in the single phase case at the same temperature: it increases by factor 3 or more at maximum calcite growth rate, then decreases due to depletion of the aqueous solution. The variation of composition of the “overgrowth” phase is confined between the curve for the effective fractionation coefficient predicted by the UUKM (upper curve) and the “bulk” coefficient at relatively high mass of the overgrowth at longer times. The specific surface area of the overgrowth phase evolves exactly as that in the single-phase case because it is related to layered aggregate particles made of the “seed” in the core and “overgrowth” outside.

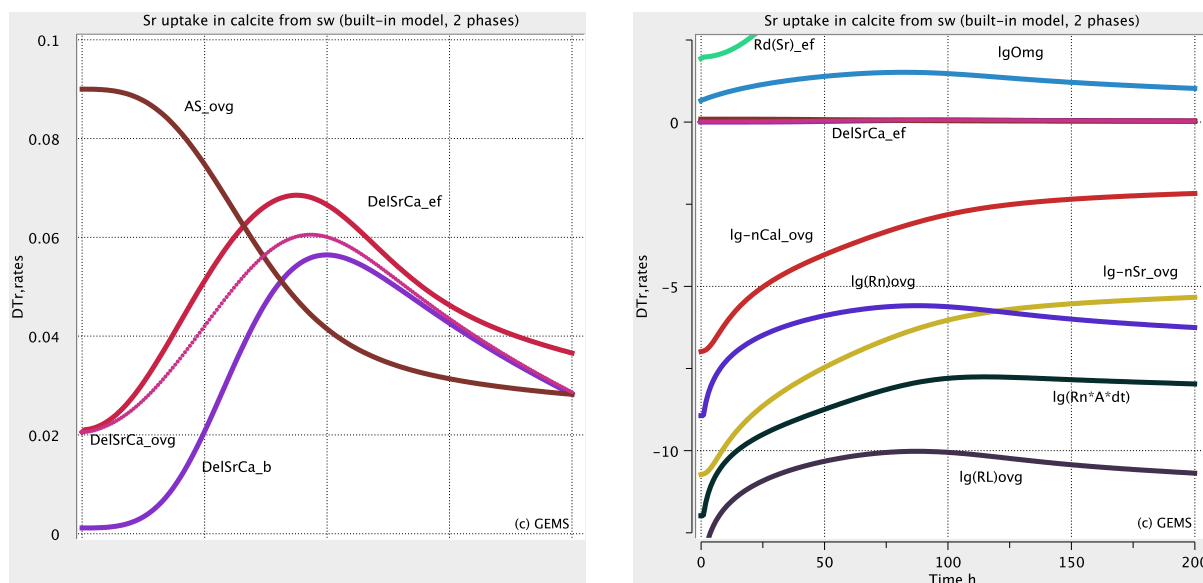


Figure 4.2.9. Simulation runs for the linked two-phase case of Sr uptake in calcite from seawater at $P = 1$ bar, $T = 25$ C, showing the effects of varying precipitation rate and seawater depletion. $DelSrCa_{ef}$: effective $\Delta_{Sr,Ca}$ (eq 18); $DelSrCa_{ovg}$: $\Delta_{Sr,Ca}$ in “overgrowth” solid solution phase; $DelSrCa_b$: bulk $\Delta_{Sr,Ca}$ in the solid; AS_{ovg} : specific surface area of the “overgrowth”; $lgOmg$: saturation index; $nCal_{ovg}$ and nSr_{ovg} : amounts of end members of the “overgrowth” phase; Rn , RL and $Rn \cdot A \cdot dt$: precipitation rates.

Conclusions and Future Work

This report summarizes the development of a new to geochemical modeling of mineral-water reaction kinetics and related uptake of radionuclides in host mineral solid solutions, verified by modeling of the experimental literature data.

Mineral precipitation with trace element incorporation is the chemical process that usually deviates from “true” aqueous-solid equilibrium. This can be modeled beyond the “complete equilibrium” concept, by invoking the principles of local- and partial equilibrium. The changes in amount and composition of an *overgrowth* phase (solid solution, surface solution, adsorbed layer) can be linked to the surface area or to volume of another, *substrate* phase (seed, sorbent), which can be itself stable or metastable with respect to aqueous solution. In the latter case, kinetic rates should be scaled by the outer surface area of the *layered composite* solid (particles).

As an extension of the GEMS3K and GEM-Selektor codes for chemical thermodynamic modelling (*Kulik et al., 2013*), some mineral reaction kinetic rate laws and uptake models for separate or metastability-linked (layered) solution phases have been implemented in the

GEM-Selektor TKinMet C++ code library. In particular, the “unified uptake kinetics model” (UUKM) for trace element incorporation upon the host mineral growth (*Thien, Kulik and Curti, 2013*) was implemented.

The TKinMet library is designed similar to the TSolMod C++ code library for models of (non-ideal) mixing in phases-solutions (Wagner et al., 2012) with the goal of keeping the GEM IPM algorithm independent of specific physicochemical features of phases and their components, while collecting all these specific parameters in Phase definition records kept in GEM-Selektor project databases. Thus, the TKinMet and the TSolMod libraries in the GEMS3K code make the application of advanced kinetic and uptake models in reactive transport simulations of complex aqueous – solid solution systems possible in repository safety scenarios.

In GEM-Selektor v.3.3 process simulations described in this report, with systems including the precipitation kinetics of portlandite and calcite, as well as the Sr and Cd uptake kinetics in calcite, some geochemically important effects are clearly demonstrated. These effects include the change of trace element uptake upon variation of precipitation rates, different temperatures, and depletion in closed- and semi-open systems. Capability of modelling such effects goes far beyond the strict limitations (e.g. constant aqueous solution composition, constant growth rate) of previously published uptake kinetics models (*Watson, 2004; DePaolo, 2011*). The test examples also show that shifts from equilibrium in the partitioning of trace elements induced by the host mineral growth are significant and extend to very slow processes at near-equilibrium conditions. In turn, this makes the GEMS codes enhanced with the TKinMet library an efficient and versatile modelling tool of potentially wide applicability in aquatic chemistry, chemical engineering, and (nuclear) waste geochemistry.

Future work should concentrate on further testing and verification of the TKinMet functionality for experimental systems that include re-crystallization of sulphates and uptake of radionuclides in them; on surface precipitation of solid solutions on goethite or other environmentally relevant substrates; on the impact of nucleation on trace element partitioning upon growth; and on studies of back-coupling and time-stepping effects and artefacts in kinetic- and reactive transport simulations.

Acknowledgement

The research leading to these results has received funding from the European Union's European Atomic Energy Community's (Euratom) Seventh Framework Program FP7-Fission-2010 under grant agreement number 269688 (CP-SKIN).

References

- DePaolo D. J. (2011). Surface kinetic model for isotopic and trace element fractionation during precipitation of calcite from aqueous solutions. *Geochimica et Cosmochimica Acta* **75**, 1039-1056.
- Dreybrodt W., Eisenlohr L., Madry B., and Ringer S. (1997). Precipitation kinetics of calcite in the system $\text{CaCO}_3\text{-H}_2\text{O-CO}_2$: The conversion to CO_2 by the slow process $\text{H}^+\text{+HCO}_3^- \rightarrow \text{CO}_2\text{+H}_2\text{O}$ as a rate limiting step. *Geochimica et Cosmochimica Acta* **49**, 2165-2180.
- Fritz B., Clement A., Amal Y., and Noguera C. (2009). Simulation of the nucleation and growth of simple clay minerals in weathering processes: The NANOKIN code. *Geochimica et Cosmochimica Acta* **73**, 1340-1358.
- Gamsjäger H., Preis W., Königsberger E., Magalhaes M. C. and Brandao P. (1999). Solid-solute phase equilibria in aqueous solution. XI. Aqueous solubility and standard Gibbs energy of cadmium carbonate. *Journal of Solution Chemistry* **28**, 711-720.
- Glynn P. and Reardon E.J. (1990). Solid-solution aqueous-solution equilibria: Thermodynamic theory and representation. *American Journal of Science* **290**, 164-201.
- Hellmann R. and Tisserand D. (2006). Dissolution kinetics as a function of the Gibbs free energy of reaction: An experimental study based on albite feldspar. *Geochimica et Cosmochimica Acta* **70**, 364-383.
- Inskeep W.P. and Bloom P.R. (1985). An evaluation of rate equations for calcite precipitation kinetics at PCO_2 less than 0.01 atm and pH greater than 8. *Geochimica et Cosmochimica Acta* **49**, 2165-2180.
- Karpov I.K., Chudnenko K.V., Kulik D.A., Avchenko O.V., and Bychinskii, V.A. (2001). Minimization of Gibbs free energy in geochemical systems by convex programming. *Geochemistry International* **39**, 1108-1119.
- Kulik D.A., Wagner T., Dmytrieva S.V., Kosakowski G., Hingerl F.F., Chudnenko K.V., and Berner U. (2013). GEM-Selektor geochemical modeling package: revised algorithm and GEMS3K numerical kernel for coupled simulation codes. *Computational Geosciences* **17**, 1-24.
- Kulik D. A., Vinograd V. L., Paulsen N., and Winkler, B. (2010). $(\text{Ca,Sr})\text{CO}_3$ aqueous-solid solution systems: From atomistic simulations to thermodynamic modelling. *Physics and Chemistry of the Earth* **35**, 217-232.
- Lasaga A.C. (1998). *Kinetic theory in the Earth sciences*. Princeton University Press, Princeton NJ.
- Lorens R. B. (1981). Sr, Cd, Mn and Co distribution coefficients in calcite as a function of calcite precipitation rate. *Geochimica et Cosmochimica Acta* **45**, 553-561.
- Madé B., Clement A., and Fritz B. (1994). *Computers and Geosciences* **20**, 1347-1363.
- Marini L., Ottonello G., Canepa M., and Cipolli F. (2000). Water-rock interaction in the Bisagno valley (Genoa, Italy): Application of an inverse approach to model spring water chemistry. *Geochimica et Cosmochimica Acta* **64**, 2617-2635.
- Mironenko M.V. and Zolotov M.Yu. (2012). Equilibrium–kinetic model of water–rock interaction. *Geochemistry International* **50**, 1-7.
- Navrotsky A. (2011). Nanoscale effects on thermodynamics and phase equilibria in oxide systems. *ChemPhysChem* **12**, 2207 – 2215.
- Nielsen L.C., De Yoreo J.J., and DePaolo D.J. (2013). General model for calcite growth kinetics in the presence of impurity ions. *Geochimica et Cosmochimica Acta* **115**, 100-114.

- Palandri J. and Kharaka Y. (2004). A compilation of rate parameters of water-mineral interaction kinetics for application to geochemical modelling. U.S.G.S. Open File Report 2004-1068, Menlo Park CA, 70 p.
- Parkhurst D.L. and Appelo C.A.J. (1999). User's guide to PHREEQC (Version 2): U.S.G.S. WRIR 99-4259, 312 p.
- Parkhurst D.L., Kipp K.L., and Charlton S.R. (2010). PHAST Version 2. U.S.G.S. Techn. Methods 6-A35, 235 p.
- Schott J., Oelkers E.H., Bénédeth P. Goddérís, Y., and François, L. (2012). Can accurate kinetic laws be created to describe chemical weathering? *Comptes Rendus Geoscience* **344**, 568-585.
- Schott J., Pokrovsky O. S., and Oelkers E. H. (2009). The link between mineral dissolution/precipitation kinetics and solution chemistry. Chapter 6 in *RiMG* **70**, 207-258.
- Scislawski A. and Zuddas P. (2010). Estimation of reactive mineral surface area during water-rock interaction using fluid chemical data. *Geochimica et Cosmochimica Acta* **74**, 6996–7007.
- Shao H., Dmytrieva S.V., Kolditz O., Kulik D.A., Pfingsten W., and Kosakowski G. (2009). Modeling reactive transport in non-ideal aqueous–solid solution system. *Applied Geochemistry* **24**, 1287-1300.
- Tadros M.E., Skalny J., and Kalyoncu, R.S. (1976). Kinetics of calcium hydroxide crystal growth from solution. *J. Colloid Interface Science* **55**, 20-24.
- Teng H.H., Dove P.M., and De Yoreo, J.J. (2000). Kinetics of calcite growth: Surface processes and relationships to macroscopic rate laws. *Geochimica et Cosmochimica Acta* **64**, 2255-2266.
- Tesoriero A. J. and Pankow J. F. (1996). Solid solution partitioning of Sr²⁺, Ba²⁺, and Cd²⁺ to calcite. *Geochimica et Cosmochimica Acta* **60**, 1053-1063.
- Thien B.M.J., Kulik D.A, and Curti E. (2013). A new approach to model uptake kinetics of trace elements in complex aqueous - solid solution systems. *Applied Geochemistry*, in revision.
- Thien B.M.J., Kulik D.A., and Curti E. (2013). Modeling trace element uptake kinetics in secondary minerals. *Procedia Earth and Planetary Science* **7**, 838-841.
- Thoenen T. (2012). The PSI/Nagra Chemical Thermodynamic Database 12/07: Compilation of updated and new data with respect to the Nagra/PSI Chemical Thermodynamic Data Base 01/01. PSI Internal Report TM-44-12-06, Paul Scherrer Institut, Villigen, Switzerland.
- Tomazic B., Mohanty R., Tadros M, and Estrin J. (1986). Crystallization of calcium hydroxide from aqueous solution. II. Observations of growth, morphology and secondary nucleation. *Journal of Crystal Growth* **75**, 339-347.
- Wadell H. (1935). Volume, shape and roundness of quartz particles. *Journal of Geology* **43**, 250–280.
- Wagner T., Kulik D.A., Hingerl F.F., and Dmytrieva S.V. (2012). GEM-Selektor geochemical modeling package: TSolMod C++ class library and data interface for multicomponent phase models. *Canadian Mineralogist* **50**, 1173-1195.
- Watson, E. B. (2004). A conceptual model for near-surface kinetic controls on the trace-element and stable isotope composition of abiogenic calcite crystals. *Geochimica et Cosmochimica Acta* **68**, 1473-1488.
- Wolthers M., Nehrke G., Gustafsson J. P., and Van Cappellen P. (2012). Calcite growth kinetics: Modeling the effect of solution stoichiometry. *Geochimica et Cosmochimica Acta* **77**, 121-134.
- Wu W. and Nancollas G.H. (1999). Determination of interfacial tension from crystallization and dissolution data: a comparison with other methods. *Advances in Colloid and Interface Science* **79**, 229-279.